

Article

# Thermal Stability of Retained Austenite and Properties of A Multi-Phase Low Alloy Steel

Zhenjia Xie \*, Lin Xiong, Gang Han, Xuelin Wang and Chengjia Shang \*

Collaborative Innovation Center of Steel Technology, University of Science and Technology Beijing, Beijing 100083, China; XiongLin\_s@163.com (L.X.); hangang@mater.ustb.edu.cn (G.H.); xuelin2076@163.com (X.W.)

\* Correspondence: zjxie@ustb.edu.cn (Z.X.); cjshang@ustb.edu.cn (C.S.); Tel.: +86-10-62332428 (Z.X. & C.S.)

Received: 16 September 2018; Accepted: 29 September 2018; Published: 9 October 2018



**Abstract:** In this work, we elucidate the effects of tempering on the microstructure and properties in a low carbon low alloy steel, with particular emphasis on the thermal stability of retained austenite during high-temperature tempering at 500–700 °C for 1 h. Volume fraction of ~14% of retained austenite was obtained in the studied steel by two-step intercritical heat treatment. Results from transmission electron microscopy (TEM) and X-ray diffraction (XRD) indicated that retained austenite had high thermal stability when tempering at 500 and 600 °C for 1 h. The volume fraction was ~11–12%, the length and width remained ~0.77 and 0.21 μm, and concentration of Mn and Ni in retained austenite remained ~6.2–6.6 and ~1.6 wt %, respectively. However, when tempering at 700 °C for 1 h, the volume fraction of retained austenite was decreased largely to ~8%. The underlying reason could be attributed to the growth of austenite during high-temperature holding, leading to a depletion of alloy contents and a decrease in stability. Moreover, for samples tempered at 700 °C for 1 h, retained austenite rapidly transformed into martensite at a strain of 2–10%, and a dramatic increase in work hardening was observed. This indicated that the mechanical stability of retained austenite decreased.

**Keywords:** thermal stability; retained austenite; multi-phase microstructure; low alloy steel

## 1. Introduction

It has been recognized that steels with retained austenite processes a good combination of strength and ductility due to the transformation-induced plasticity (TRIP) effect of retained austenite [1–3]. Retained austenite has become an essential component in the development of new-generation, advanced, high-strength steels in the automobile industry. In addition, stable retained austenite has been suggested to be helpful for the improvement of low-temperature toughness by lowering ductile–brittle transition temperature (DBTT). Much attention has been paid to the development of high-strength, high-toughness steels via the introduction of stable retained austenite. Significant progress has been made. In quenched and tempered nickel-rich (5–9 wt %) steels, high toughness at a cryogenic temperature of –196 °C was achieved due to the existence of stable film-like retained austenite along grain boundaries and martensite laths [4,5]. By combination of the TRIP effect and the martensite aging effect, an ultra-high strength (1.5 GPa) with a good combination of ductility and toughness was obtained in maraging steel [6]. In ultra-fine super-bainite steels, a very high strength (2.5 GPa) and good toughness was achieved by obtaining stable retained austenite [7].

In recent years, retained austenite has been introduced to low-carbon (<0.1 wt %), low-alloy (~2–3 wt % Mn) steels [8,9]. A high yield strength (~500–700 MPa) with excellent ductility and high toughness at low temperatures was obtained with a multi-phase microstructure containing a stable film-like retained austenite [10,11], which has great potential for structural engineering

applications. However, retained austenite is inevitably exposed to high temperatures in certain processes, such as galvanization, the heat effect zone during welding, and fire-resistant applications [12]. This brings about risks due to the deteriorated stability of retained austenite. This suggests that retained austenite decomposes into thermodynamically stable ferrite and cementite, leading to a sudden deterioration in toughness and an increase in DBTT, known as tempering embrittlement [13–15]. Therefore, understanding the thermal stability of retained austenite upon tempering is an essential topic to design low-carbon, low-alloy steel with retained austenite.

In this work, a multi-phase microstructure containing retained austenite was produced via two-step intercritical heat treatment in a low-carbon, low-alloy steel, as our previous work [8]. The influence of tempering at 500–700 °C on the multi-phase microstructure was studied by scanning electron microscopy (SEM), transmission electron microscopy (TEM), and X-ray diffraction (XRD) with particular emphasis on the thermal stability of retained austenite. Moreover, the effect of the stability of retained austenite on properties was investigated.

## 2. Experimental Material and Procedure

The experimental steel was designed with a chemical composition of 0.1C-2.0Mn-1.5(Si + Al)-1.0Cu-1.0Ni-0.3Mo. High silicon and aluminum was designed to suppress carbide formation and increase the stability of the retained austenite. Molybdenum was added mainly for solid-solution strengthening and retarding recovery during high-temperature tempering [12]. The experimental steel was smelted by a 50 kg vacuum induction furnace (ZGXL-0.05, Jinzhou, China), forged into rod diameter of 14 mm. In order to eliminate the effect of forging, the forged rods were held at 980 °C for 20 min, and water was then quenched to room temperature. The two-step intercritical heat treatment and subsequent tempering process are illustrated in Figure 1. The quenched rods were re-heated to 780 °C for 30 min, and water cooled to ambient temperature. The rods were then held at 680 °C for 30 min, and air cooled to room temperature. Finally, these heat-treated samples were tempered at 500, 600, and 700 °C for 1 h to investigate the thermal stability of retained austenite and the effect on mechanical properties.

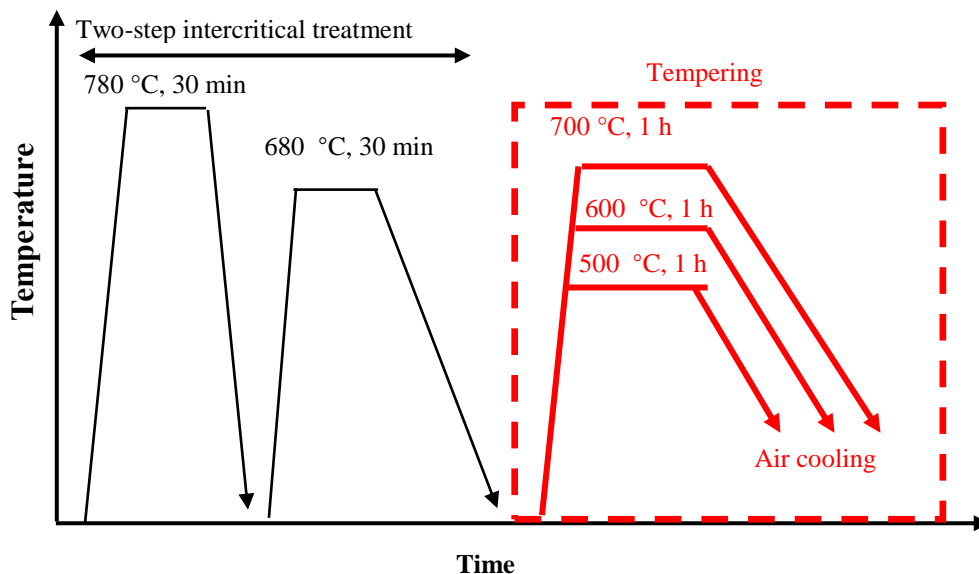


Figure 1. Schematic diagram of the heat treatment in this work.

Standard tensile tests with a diameter of 5 mm and gauge length of 25 mm were conducted at room temperature on longitudinal samples, machined according to ASTM using computerized universal testing system at a strain rate of  $1 \times 10^{-3} \text{ s}^{-1}$ . SEM samples with a dimension of  $\phi 14 \times 4 \text{ mm}$  were cut from the edge of tensile specimens for different tempering temperatures.

After mechanical grinding and polishing, SEM samples were etched with 3% nital and characterized by a ZEISS ULTRA-55 field emission scanning electron microscope (FE-SEM, ZEISS, Jena, Germany) operated at 20 kV. After SEM observation, samples were ground and electron-polished to determine the volume fraction of the retained austenite by X-ray diffraction (XRD). The solution was ethanol/perchloric acid/glycerol = 8.5:1:0.5, with a constant voltage of 18 V and a current of ~1.2 A. Quantitative assessments of retained austenite were carried out by XRD (Smartlab 9KW, Tokyo, Japan) using  $\text{CuK}\alpha$  radiation. The volume fraction of retained austenite was estimated by measuring the peak intensity of  $(200)\alpha$ ,  $(211)\alpha$ ,  $(200)\gamma$ ,  $(211)\gamma$ , and  $(311)\gamma$ . Moreover, electron back-scattered diffraction (EBSD, EDAX Inc., Hikari, NJ, USA) in the SEM operated at 20 kV was also used to study the evolution of retained austenite with different tensile strains. The step size was 0.1  $\mu\text{m}$ . Standard 3 mm TEM discs were prepared by a twin-jet polishing technique using an electrolyte of 10% perchloric acid and 90% ethanol. Microstructures after tensile tests were observed in a JEOL JEM-2100FS TEM (JEOL, Tokyo, Japan) with an energy dispersive X-ray spectrometer (EDS) operated at 200 kV.

### 3. Results and Discussion

Figure 2 presents the SEM microstructure for the experimental steel before and after tempering at 500–700 °C. After two-step intercritical heat treatment, a multi-phase microstructure consisting of intercritical ferrite, martensite/retained austenite was obtained, as shown in Figure 2a. The microstructural development and stabilization of retained austenite was elucidated in our previous studies [8–11]. It was suggested that, during intercritical annealing at 780 °C, reverted austenite formed uniformly along prior austenite grain boundaries and martensite matrix lath boundaries. With the growth of reverted austenite during holding, alloying elements including C, Mn, and Ni that are partitioned into the reverted austenite form an adjacent annealed martensite matrix, leading to a mixture microstructure of alloying-enriched austenite and alloying-depleted annealed martensite (intercritical ferrite). Due to the high hardenability of the alloying-enriched reverted austenite, the austenite transformed to martensite during the subsequent water cooling. Hence, a dual-phase microstructure consisting of intercritical ferrite and martensite was obtained by the first intercritical annealing at 780 °C. By the second step, intercritical annealing at 680 °C, reverted austenite formed at the alloying-enriched martensite, and was further enriched by C, Mn, and Ni. Because of the high enrichment of alloying elements and fine grain size of reverted austenite, retained austenite was obtained, leading to a multi-phase microstructure consisting of intercritical ferrite, martensite, and retained austenite. After tempering at 500–700 °C for 1 h, there is no obvious change in the multi-phase microstructure consisting of intercritical ferrite and tempered martensite/retained austenite. The multi-phase microstructure remained a lamina morphology. It indicated that the multi-phase microstructure had good thermal stability upon high-temperature tempering.

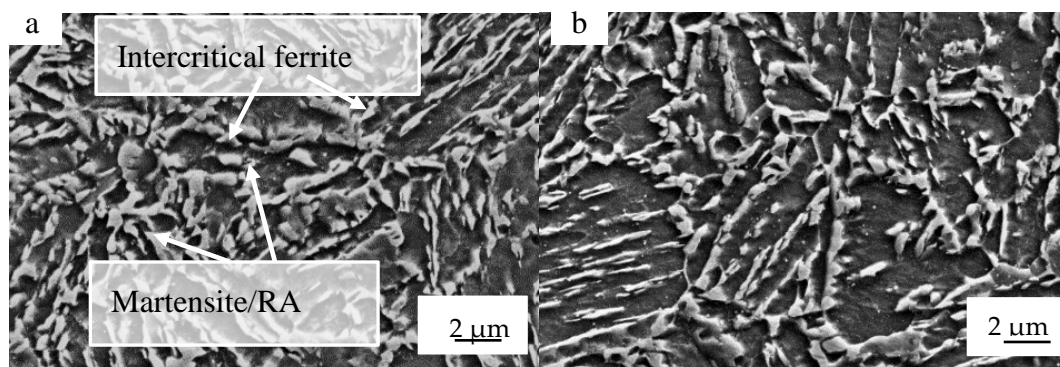
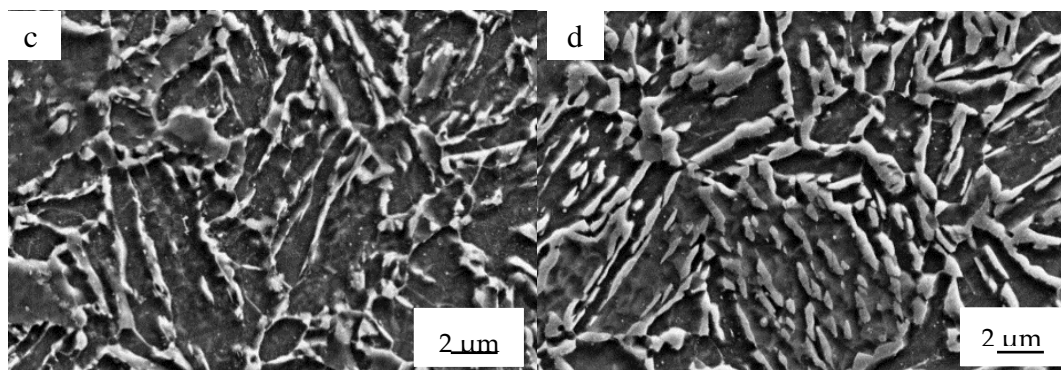
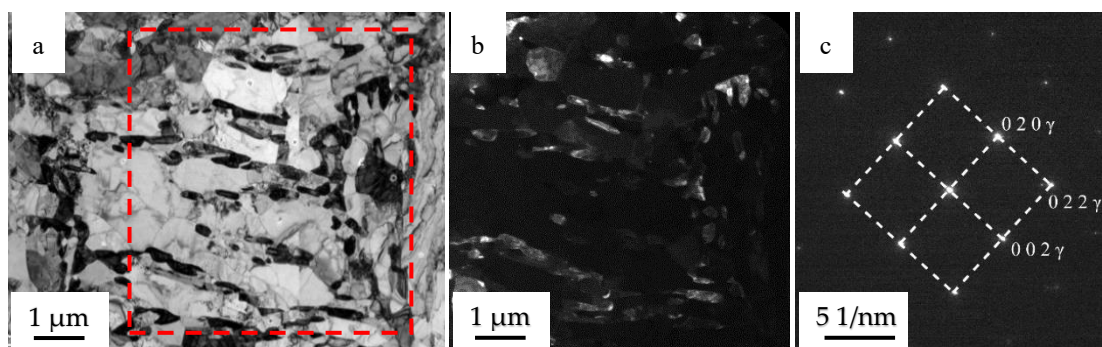


Figure 2. Cont.



**Figure 2.** SEM images of the studied steel before (a) and after tempering at different temperatures: (b) 500 °C, (c) 600 °C, (d) 700 °C.

The detailed microstructure of retained austenite for samples before and after tempering at 500–700 °C was characterized by TEM. Figure 3 presents the TEM microstructure of sample after the two-step intercritical treatment without the third step of tempering. The TEM bright-field image of microstructure revealed that retained austenite (the dark areas in Figure 3a) manifested a film-like morphology trapped between ferritic matrix laths and presented a granular shape along prior austenite grain boundaries, as did the corresponding dark-field image for retained austenite (Figure 3b) and selected area diffraction pattern (SADP) analysis with an austenite zone axis of  $[1\ 0\ 0]$  (Figure 3c). After tempering at 500 °C, the retained austenite remained thermodynamically stable within the matrix, and no decomposition of retained austenite into nano-sized carbides and ferrite was observed, as shown in Figure 4a,b. SADP analysis results (Figure 4c) confirmed that the dark areas in the TEM bright-field image (Figure 4a) and light areas in the TEM dark-field image (Figure 4b) were face-centered-cubic (FCC) retained austenite under an austenite zone axis of  $[1\ 1\ 0]$ . When the tempering temperature was up to 600 or 700 °C, the multi-phase microstructure of the studied steel was also thermally stable. No retained austenite decomposed into carbides or ferrite, as shown in Figure 4d,e, respectively. Retained austenite kept in film-like morphology within the ferritic laths and granular type at prior austenite grain boundaries.



**Figure 3.** (a) Bright-field TEM images of retained austenite in the studied steel after the two-step intercritical treatment before tempering; (b) dark-field TEM images of retained austenite for the red rectangle area; (c) corresponding diffraction pattern of retained austenite under the zone axis of  $[1\ 0\ 0]$ .

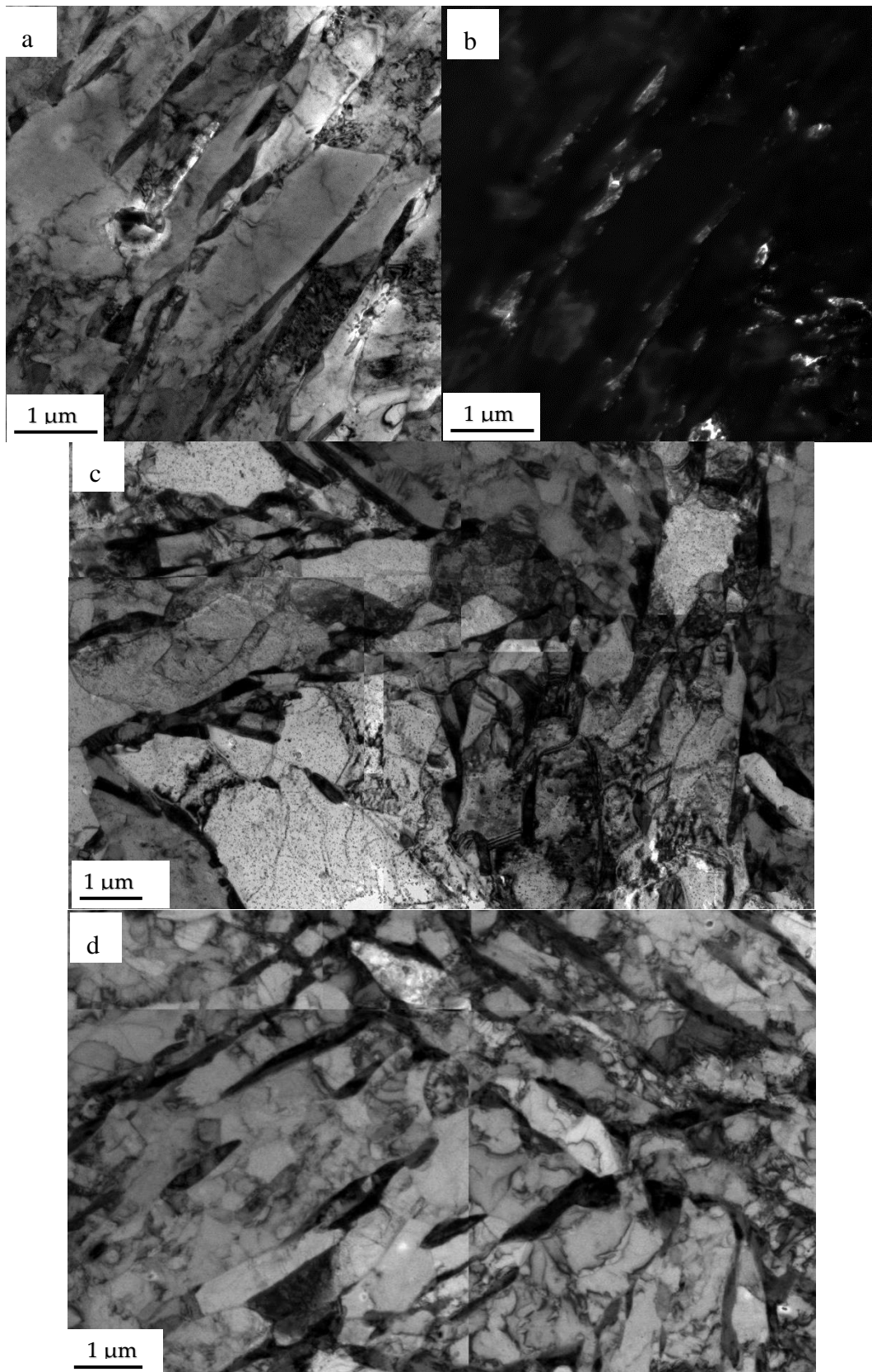


**Figure 4.** (a,c,d) Bright-field TEM images of retained austenite (RA) for samples tempered at 500, 600, and 700 °C, respectively; (b) dark-field images of RA in (a).

The volume fraction of retained austenite in experimental steel before and after tempering at 500–700 °C was determined by XRD, and the obtained XRD spectra and calculated results are presented in Figure 5. The specimen before tempering contained the maximum volume fraction of ~14%. After tempering at 500 and 600 °C, the volume fraction of retained austenite slightly decreased to ~12 and 11%, respectively. It can be deduced that retained austenite in the studied steel obtained by the two-step intercritical treatment had good thermal stability upon tempering at 500–600 °C. However, after tempering at 700 °C, the volume fraction of retained austenite was reduced largely to ~8%. The decrement in volume fraction of retained austenite should be attributed to the growth of austenite during holding at a high-temperature tempering of 700 °C, leading to a decreased chemical stability of austenite due to the depleted alloying elements and grain coarsening.

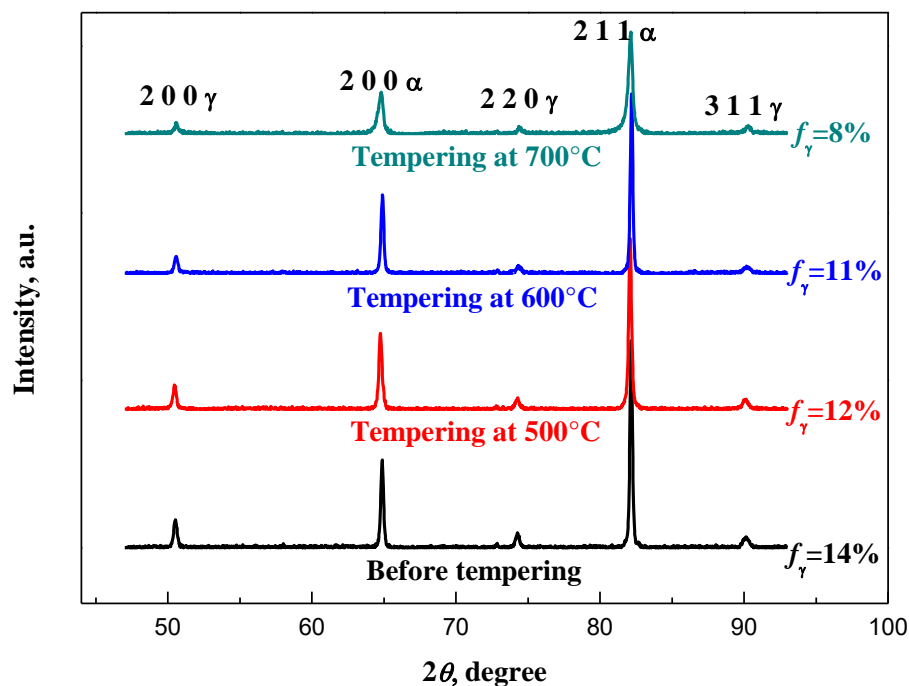


**Figure 5.** XRD spectra for samples before and after tempering at 500–700 °C.

The dimension in length and width of austenite areas was measured from corresponding TEM micrographs of samples before and after different tempering treatments. Each data was obtained from at least 50 measurements, and the obtained results are plotted in Figure 6. It can be seen that the length and width of austenite for sample before tempering and samples tempered at 500 and 600 °C are similar, and they are ~0.77 and ~0.21  $\mu\text{m}$ , respectively. After tempering at 700 °C, the dimension of austenite areas largely increased, the length and width were up to ~1.7 and 0.28  $\mu\text{m}$ , respectively. In addition, EDS analysis was carried out to detect concentrations of the alloying elements (Mn and Ni) in austenite. Each data was determined from at least 10 measurements, and the analyzed results are presented in Figure 6. After the two-step intercritical treatment, manganese and nickel in austenite were enriched to as high as ~6.8 and 1.7 wt %, respectively. After tempering at 500 and 600 °C, the concentration of manganese and nickel in austenite remained similar to the sample before tempering, ~6.2–6.6 and ~1.6 wt %, respectively, whereas the concentrations of manganese and nickel for samples tempered at 700 °C decreased to ~5.4 and ~1.4 wt %, respectively.

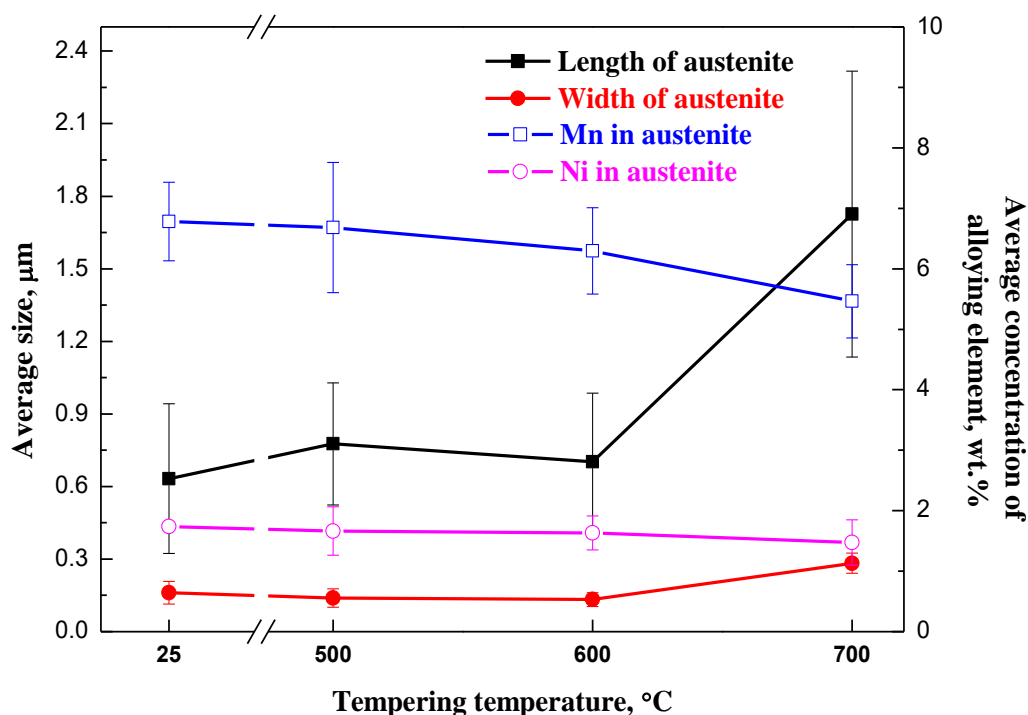


**Figure 6.** Statistic results of dimension (solid symbol) and alloying elements (Mn and Ni) concentration (blank symbol) of retained austenite by TEM images for samples before and after tempering at 500–700 °C.

On the basis of our previous studies [8,11] on microstructure evolution and mechanism of retained austenite during the two-step intercritical treatment, the thermal stability of retained austenite in the present study upon tempering can be interpreted as follows. It was revealed that the first step of intercritical annealing decreased  $A_{c1}$  temperature (designated as  $A_{c1}'$  temperature) of the experimental steel due to the enrichment of alloying elements in martensite. Therefore, reverted austenite was able to form at a relative low temperature in the range of  $A_{c1}'-A_{c1}$  and was stabilized and retained because of a further enrichment of alloy content and fine grain size [16–18]. When the third tempering temperature (500 and 600 °C) was lower than  $A_{c1}'$ . Retained austenite was stable and no further growth was observed in this work. When the tempering temperature (700 °C) was higher than  $A_{c1}'$ , an obvious growth of austenite was observed both in thickness and length. With the growing of austenite, the alloy content in austenite was depleted, and the stability of austenite was thus reduced. Furthermore, the increase in grain size of austenite also largely decreased the stability of austenite. As a result, some retained austenite developed into martensite and the volume fraction of retained austenite decreased to 8% after tempering at 700 °C for 1 h in this study.

On the other hand, retained austenite exhibited high thermal stability on tempering at 500 and 600 °C, and no obvious decomposition into ferrite and carbides was observed. This was different from the retained austenite in conventional CMnSiAl TRIP steel as reported in [18], in which retained austenite decomposed into ferrite and carbides when tempered at 300–500 °C and the kinetics of the decomposition was accelerated when the tempering temperature was increased. It has been suggested that the thermal stability of retained austenite is strongly affected by carbon content [19,20]. It was found that, because of its lower carbon content, large block-type retained austenite had a high thermal stability compared to small film-type retained austenite [21], leading to a lower driving force for carbide formation. Based on our previous study using atom probe tomography with a similar steel by this two-step intercritical treatment, the carbon content in the retained austenite was ~0.4 wt % [9]. The carbon concentration was much lower than the ~1 wt % in the retained austenite in the conventional TRIP steel [22,23]. In addition, high silicon and aluminum (~1.5 wt % in total) were added

in the studied steel, which can suppress carbide formation during tempering. Therefore, the high thermal stability of retained austenite was obtained when tempered at 500 and 600 °C.

Uniaxial tensile tests were carried out at room temperature to reveal the mechanical stability of retained austenite and its effect on ductility for samples before and after tempering. The received stress–strain curves are plotted in Figure 7. From these engineering stress–strain curves, yield strength, tensile strength, uniform and total elongation were determined. As seen from Figure 7, samples before and after tempering at 500 and 600 °C possessed similar stress–strain behavior, exhibiting a yield strength of ~649–664 MPa, a tensile strength of ~766–773 MPa, and a high ductility (a uniform elongation of ~18–20% and a total elongation of ~35–36%). This finding implies that retained austenite after it is tempered at 500 and 600 °C has a mechanical stability similar to that before tempering. Unlike the thermal stability of retained austenite, the mechanical stability is largely dependent on chemical composition and the grain size of retained austenite, shape, and distribution [24], partitioning of strain between phases [25,26]. The similar mechanical stability could be attributed to their similar chemical composition and grain size for samples before and after tempering at 500 and 600 °C. However, samples tempered at 700 °C had a different stress–strain behavior, as shown in Figure 7. For samples tempered at 700 °C, it manifested a low yield strength of ~580 MPa and a high tensile strength of ~877 MPa, presenting rapid work hardening to fracture. The low yield stress could be attributed to severe recovery due to high-temperature aging. The rapid work hardening route may be caused by the decrease in the mechanical stability of retained austenite due to the low alloy content, leading to dramatic transformations to martensite during early strain.

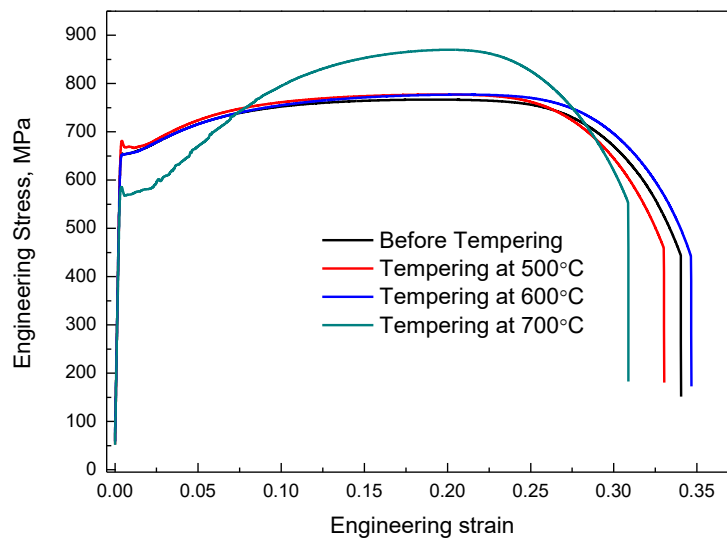


**Figure 7.** Engineering stress–strain curves for samples before and after tempering at 500–700 °C.

In the present work, EBSD studies were conducted to investigate the mechanical stability of retained austenite for samples tempered at 700 °C. The analyzed EBSD results are presented in Figure 8a–c, corresponding to specimens after strains of 2, 5, and 10%. As seen in Figure 8a, after an early stage of deformation ( $\epsilon = 2\%$ ), the retained austenite was uniformly distributed between matrix laths in film-like shape and at grain boundaries in blocky morphology. Dark areas, which were considered hard martensite [27] with a low band contrast (BC) value, were observed nearby both types of retained austenite (film-like type and block type). This finding implies that the retained austenite was partially transformed into martensite at low strain. Similar results were reported in conventional TRIP steel [24]. When strain was increased to 5% (Figure 8b), the martensite (dark area) increased, and the retained austenite decreased. Quantitative analysis results indicated that ~50% of the retained austenite transformed into martensite after a strain of 5% in comparison with the sample after a strain of 2%. When strain was further increased to 10%, almost all retained austenite was transformed into martensite, and little of the retained austenite at the grain boundaries remained,

as shown in Figure 8c. This implies that the retained austenite in samples tempered at 700 °C presented a relative low mechanical stability compared to those in conventional TRIP steel [24]. Therefore, a dramatic increase in work hardening was observed at a strain of 2–10%. Nevertheless, by modifying work hardening behavior due to strain-induced martensite transformation of retained austenite, high ductility (a uniform elongation of ~19% and a total elongation of ~33%) was obtained.

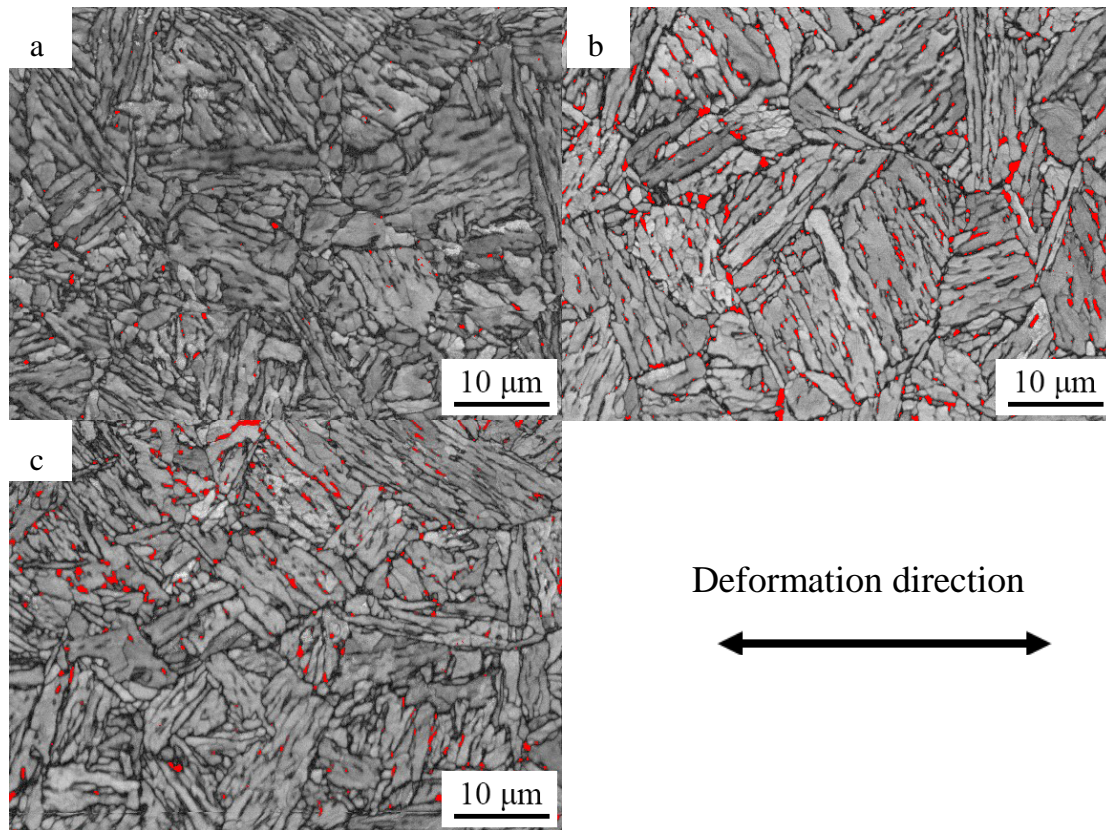


**Figure 8.** EBSD micrographs of retained austenite for samples tempered at 700 °C at different tensile strains: (a) strain  $\epsilon = 2\%$ , (b) strain  $\epsilon = 5\%$ , (c) strain  $\epsilon = 10\%$  (red corresponds to retained austenite).

#### 4. Conclusions

In this study, multi-phase microstructure consisting of intercritical ferrite, martensite, and ~14% volume fraction retained austenite was obtained by a novel two-step intercritical treatment in 0.1C-2.0Mn-1.5(Si, Al)-1.0Cu-1.0Ni steel. Tempering effects on microstructure evolution, the stability of retained austenite, and the resultant properties were carefully investigated using SEM, TEM, XRD, and EBSD. The results and conclusions are summarized as follows:

(1) Retained austenite obtained by two-step intercritical treatment was thermally stable when tempering at 500 and 600 °C for 1 h. The volume fraction of retained austenite was slightly decreased from ~14 to ~11–12%, and alloy contents in retained austenite and size in length and width remained similar to that before tempering. In addition, the experimental steel after tempering at 500 and 600 °C had similar stress–strain behavior to that before tempering. This implies that there was no obvious change in the mechanical stability.

(2) The volume fraction of the retained austenite was decreased largely to ~8% after tempering at 700 °C for 1 h. Results from TEM characterization suggest that the underlying reason could be attributed to the rapid growth of austenite during holding at high temperature. In addition, the retained austenite rapidly transformed into martensite at a strain of 2–10%, and a dramatic increase in work hardening was observed. This indicated that the mechanical stability of retained

austenite was decreased. Nevertheless, by modifying work hardening behavior due to strain-induced martensite transformation of retained austenite, high ductility (a uniform elongation of ~19% and a total elongation of ~33%) was obtained.

**Author Contributions:** Z.X. analyzed the results and wrote the draft; L.X. and G.H. performed the experiments; X.W. reviewed the draft; C.S. designed and supervised the experiments.

**Funding:** This research was funded by the National Natural Science Foundation of China (No. 51701012) and the Fundamental Research Funds for the Central Universities (No. FRF-TP-17-004A1).

**Conflicts of Interest:** The authors declare no conflict of interest.

## References

1. Sugimoto, K.I.; Kobayashi, M.; Hashimoto, S.I. Ductility and strain-induced transformation in a high-strength transformation-induced plasticity-aided dual-phase steel. *Metall. Mater. Trans. A* **1992**, *23*, 3085–3091. [[CrossRef](#)]
2. Raabe, D.; Ponge, D.; Dmitrieva, O.; Sander, B. Nanoprecipitate-hardened 1.5 GPa steels with unexpected high ductility. *Scr. Mater.* **2009**, *60*, 1141–1144. [[CrossRef](#)]
3. Speer, J.; Matlock, D.K.; De Cooman, B.C.; Schroth, J.G. Carbon partitioning into austenite after martensite transformation. *Acta Mater.* **2003**, *51*, 2611–2622. [[CrossRef](#)]
4. Kim, J.I.; Syn, C.K.; Morris, J.W. Microstructural sources of toughness in QLT-treated 5.5 Ni cryogenic steel. *Metall. Trans. A* **1983**, *14A*, 93–103. [[CrossRef](#)]
5. Fultz, B.; Kim, J.I.; Kim, Y.H.; Kim, H.J.; Fior, G.O.; Morris, J.W. The stability of precipitated austenite and the toughness of 9Ni steel. *Metall. Trans. A* **1985**, *16A*, 2237–2249. [[CrossRef](#)]
6. Raabe, D.; Ponge, D.; Dmitrieva, O.; Sander, B. Designing ultrahigh strength steels with good ductility by combining transformation induced plasticity and martensite aging. *Adv. Eng. Mater.* **2009**, *11*, 547–555. [[CrossRef](#)]
7. Caballero, F.G.; Bhadeshia, H.K.D.H. Very strong bainite. *Curr. Opin. Solid State Mater. Sci.* **2004**, *8*, 251–257. [[CrossRef](#)]
8. Zhou, W.H.; Guo, H.; Xie, Z.J.; Wang, X.M.; Shang, C.J. High strength low-carbon alloyed steel with good ductility by combining the retained austenite and nano-sized precipitates. *Mater. Sci. Eng. A* **2013**, *587*, 365–371. [[CrossRef](#)]
9. Xie, Z.J.; Shang, C.J.; Subramanian, S.V.; Ma, X.P.; Misra, R.D.K. Atom probe tomography and numerical study of austenite stabilization in a low carbon low alloy steel processed by two-step intercritical heat treatment. *Scr. Mater.* **2017**, *137*, 36–40. [[CrossRef](#)]
10. Zhou, W.H.; Wang, X.L.; Venkatsurya, P.K.C.; Guo, H.; Shang, C.J.; Misra, R.D.K. Structure–mechanical property relationship in a high strength low carbon alloy steel processed by two-step intercritical annealing and intercritical tempering. *Mater. Sci. Eng. A* **2014**, *607*, 569–577. [[CrossRef](#)]
11. Xie, Z.J.; Yuan, S.F.; Zhou, W.H.; Yang, J.R.; Guo, H.; Shang, C.J. Stabilization of retained austenite by the two-step intercritical heat treatment and its effect on the toughness of a low alloyed steel. *Mater. Des.* **2014**, *59*, 193–198. [[CrossRef](#)]
12. Wan, R.C.; Sun, F.; Zhang, L.T.; Shan, A.D. Effects of Mo on high-temperature strength of fire-resistant steel. *Mater. Des.* **2012**, *35*, 335–341. [[CrossRef](#)]
13. Sarikaya, M.; Jhingan, A.K.; Thomas, G. Retained austenite and tempered martensite embrittlement in medium carbon steels. *Metall. Trans. A* **1983**, *9A*, 1121–1133. [[CrossRef](#)]
14. Thomas, G. Retained austenite and tempered martensite embrittlement. *Metall. Trans. A* **1978**, *9A*, 439–450. [[CrossRef](#)]
15. Xie, Z.J.; Fang, Y.P.; Han, G.; Guo, H.; Misra, R.D.K.; Shang, C.J. Structure–property relationship in a 960 MPa grade ultrahigh strength low carbon niobium–vanadium microalloyed steel: The significance of high frequency induction tempering. *Mater. Sci. Eng. A* **2014**, *618*, 112–117. [[CrossRef](#)]
16. Umamoto, M.; Owen, W.S. Effects of austenitizing temperature and austenite grain size on the formation of athermal martensite in an iron-nickel and an iron-nickel-carbon alloy. *Metall. Trans.* **1974**, *5*, 2041–2046. [[CrossRef](#)]

17. Yang, H.S.; Bhadeshia, H.K.D.H. Austenite grain size and the martensite-start temperature. *Scr. Mater.* **2009**, *60*, 493–495. [[CrossRef](#)]
18. Yen, H.W.; Ooi, S.W.; Eizadjou, M.; Breen, A.; Huang, C.Y.; Bhadeshia, H.K.D.H.; Ringer, S.P. Role of stress-assisted martensite in the design of strong ultrafine-grained duplex steels. *Acta Mater.* **2015**, *82*, 100–114. [[CrossRef](#)]
19. Park, H.S.; Seol, J.B.; Lim, N.S.; Kim, S.; Park, C.G. Study of the decomposition behavior of retained austenite and the partitioning of alloying elements during tempering in CMnSiAl TRIP steels. *Mater. Des.* **2015**, *82*, 173–180. [[CrossRef](#)]
20. Park, H.S.; Han, J.C.; Lim, N.S.; Seol, J.B.; Park, C.G. Nano-scale observation on the transformation behavior and mechanical stability of individual retained austenite in CMnSiAl TRIP steels. *Mater. Sci. Eng. A* **2015**, *627*, 262–269. [[CrossRef](#)]
21. Podder, A.S.; Lonardelli, I.; Molinari, A.; Bhadeshia, H.K.D.H. Thermal stability of retained austenite in bainitic steel: an in situ study. *Proc. R. Soc. A Math. Phys. Eng. Sci.* **2011**, *467*, 3141–3156. [[CrossRef](#)]
22. Edmonds, D.V.; He, K.; Rizzo, F.C.; De Cooman, B.C.; Matlock, D.K.; Speer, J.G. Quenching and partitioning martensite—A novel steel heat treatment. *Mater. Sci. Eng. A* **2006**, *438–440*, 25–34. [[CrossRef](#)]
23. Zwaag, S.V.D.; Zhao, L.; Kruijver, S.O.; Sietsma, J. Thermal and mechanical stability of retained austenite in aluminum-containing multiphase TRIP steels. *ISIJ Int.* **2002**, *42*, 1565–1570. [[CrossRef](#)]
24. Xie, Z.J.; Ren, Y.Q.; Zhou, W.H.; Yang, J.R.; Shang, C.J.; Misra, R.D.K. Stability of retained austenite in multi-phase microstructure during austempering and its effect on the ductility of a low carbon steel. *Mater. Sci. Eng. A* **2014**, *603*, 69–75. [[CrossRef](#)]
25. Ryu, J.H.; Kim, D.I.; Kim, H.S.; Bhadeshia, H.K.D.H.; Suh, D.W. Strain partitioning and mechanical stability of retained austenite. *Scr. Mater.* **2010**, *63*, 297–299. [[CrossRef](#)]
26. Chatterjee, S.; Wang, H.S.; Yang, J.R.; Bhadeshia, H.K.D.H. Mechanical stabilisation of austenite. *Mater. Sci. Technol.* **2006**, *22*, 641–644. [[CrossRef](#)]
27. Santofimia, M.J.; Zhao, L.; Sietsma, J. Microstructural evolution of a low-carbon steel during application of quenching and partitioning heat treatments after partial austenitization. *Metall. Mater. Trans. A* **2009**, *40A*, 46–57. [[CrossRef](#)]



© 2018 by the authors. Licensee MDPI, Basel, Switzerland. This article is an open access article distributed under the terms and conditions of the Creative Commons Attribution (CC BY) license (<http://creativecommons.org/licenses/by/4.0/>).